Title: A QCM-D and SAXS Study of the Interaction of Functionalised Lyotropic Liquid Crystalline Lipid Nanoparticles with siRNA

Authors: Behnoosh Tajik-Ahmadabad, MSc; Adam Mechler, PhD; Benjamin W Muir, PhD; Keith McLean, PhD; Tracey M Hinton, PhD; Frances Separovic, PhD; Anastasios Polyzos, PhD

To be cited as: ChemBioChem 10.1002/cbic.201600613

Link to VoR: https://doi.org/10.1002/cbic.201600613

A QCM-D and SAXS Study of the Interaction of Functionalised Lyotropic Liquid Crystalline Lipid Nanoparticles with siRNA

Behnoosh Tajik-Ahmadabad[a,b], Adam Mechler[c], Benjamin W. Muir[b], Keith McLean[b], Tracey M. Hinton[d], Frances Separovic[a] and Anastasios Polyzos[a,b]

Abstract: Biophysical studies were undertaken to investigate the binding and release of short interfering ribonucleic acid (siRNA) from lyotropic liquid crystalline lipid nanoparticles (LNPs) using a quartz crystal microbalance (QCM). These carriers are based on phytantriol (Phy) and a cationic lipid, DOTAP (1, 2–dioleoyl–3 trimethylammonium propane). The non-lamellar phase LNPs were tethered to the surface of the QCM chip for analysis based on biotin-neutravidin binding, which enabled the controlled deposition of siRNA-LNP complexes with different lipid/siRNA charge ratios on a QCM-D crystal sensor. The binding and release of biomolecules such as siRNA from LNPs was demonstrated to be reliably characterized using this technique. Essential physicochemical parameters of the cationic LNP/siRNA lipoplexes, such as particle size, lyotropic mesophase behavior, cytotoxicity, gene silencing and uptake efficiency, were also assessed. The SAXS data show that upon lowering the pH to 5.5, the structure of lipoplexes did not change, indicating that the acidic conditions of the endosome were not a significant factor in the release of siRNA from the cationic lipidic carriers.

Introduction

In recent years, the importance of lyotropic liquid crystalline mesophases (LLCs) especially inverse bicontinous cubic liquid crystalline phases (Q_{II}) as bioactive delivery vehicles has increased significantly [1-4]. The bicontinous cubic phase, which was first recognized by Luzzati *et al.* [5], consists of a single continuous lipid bilayer that separates two bicontinuous but nonintersecting water channels, and hence is well suited to encapsulation of small molecules [6].

A dispersed form of inverse bicontinous cubic lyotropic liquid crystalline phase lipids are the so called cubosomes that can be formed in aqueous media of non-ionic amphiphiles such as phytantriol and glycerol monooleate (GMO). The self-assembly of these species results in the formation of a nonporous 3D network of water-amphiphile channels that creates an internal interfacial area of approximately 400 m^2/g of amphiphile [5-9]. Depending on the environment three common cubic phases may be observed: the primitive (*Im3m*), the diamond (*Pn3m*) and the gyroid phases (*Ia3d*) [1]. Cubosomes are typically formed by dispersion of bulk cubic phase using high shear energy methods such as sonication and homogenisation followed by addition of an agent to impart colloidal stabilisation to prevent their re-flocculation upon dispersion [10-12].

Lipid-based nanoparticles including cubosomes have long been used to deliver biologically active molecules including drugs, DNA, and more recently, siRNA *in vivo*, owing to the potential to promote membrane fusion and subsequently release of the payload over a sustained period of time [13-19]. Compared to other siRNA delivery systems, such as liposomes and polymeric delivery vehicles, cubosomes have a much higher interfacial area (high surface-to-volume ratio) that improves the encapsulation efficiency of drugs. Moreover, the ability to tune the water channel size provides a capability for multi-drug nano encapsulation [20-25]. They also tolerate many additives (lipids and proteins) without disruption of the cubic structure] and are able to protect the cargo against chemical and enzymatic degradation [16, 21, 26].

Nucleic acid therapy and, in particular, gene silencing by RNA interference (RNAi) is a promising new therapeutic strategy for viral infections, cancer, and genetic disorders [27, 28]. It relies on blocking the expression of specific disease related proteins through the inactivation of mRNA with specific short interfering RNA fragments (siRNA), that are

[a] B. Tajik-Ahmadabad, Prof. F. Separovic, Dr A. Polyzos
School of Chemistry, Bio21 Institute, The University of Melbourne, Melbourne VIC 3010, Australia
E-mail: fs@unimelb.edu.au ; anastasios.polyzos@unimelb.edu.au

[b] Dr B.W. Muir, Dr K. McLean, Dr A. Polyzos
CSIRO, Manufacturing Flagship, Clayton VIC 3168, Australia

[c] Dr A. Mechler
La Trobe Institute for Molecular Science La Trobe University, Bundoora, VIC 3083, Australia

[d] Dr T.M. Hinton
CSIRO Health and Biosecurity, Australian Animal Health Laboratory, Geelong, VIC 3220, Australia

introduced into the cell as a therapeutic agent. Naked siRNA, due to its anionic nature, is not able to passively cross cellular membranes to reach its site of action in the cytoplasm, and needs a safe and effective delivery system that actively promotes cellular internalization and endosomal escape [29-31]. A number of reviews [30, 32-34] emphasize the promising properties of lipid vectors especially cationic lipid vectors for siRNA delivery. The commonly used cationic lipids for siRNA delivery are DOTAP (1, 2–dioleoyl–3 trimethylammonium propane), DODAB (1, 2–dioleoyl–3–dimethylammonium propane), DOTMA (1, 2–di–O octadecenyl–3–trimethylammonium propane), DDAB (dimethyl dioctadecyl ammonium) and Lipofectin. DOTAP and analogues together with dioleoyl phosphatidylethanolamine (DOPE) have been shown to facilitate siRNA delivery [35]. Although the complex of cationic lipid-siRNA (lipoplex) systems have emerged as attractive vehicles for siRNA [35], they need further development in terms of transfection efficiency, toxicity and stability in serum. Furthermore, the less than optimal encapsulation efficiency of lipid-based liposomes limits performance, i.e., considerable free siRNA remains unbound in solution.

Given that the lipoplex structure has a significant influence on the transfection efficiency of genetic material to cells and fusogenicity contributes to cytoplasmic delivery of siRNA, fusogenic lipids are being used in nanocarriers formulations. Lipidic cubosome delivery systems have been proposed to possess efficient fusogenic properties independent of membrane charge density and are able to promote endosomal escape and improve siRNA delivery to the cells [36-40]. They can tolerate many additives (lipids and proteins) without disruption of cubic structure [20]. Leal *et al.* [37] established that cubic phases could be used for siRNA delivery with improved endosomal escape and cytoplasmic delivery of lipid-siRNA complexes together with low toxicity. Furthermore, the positively charged cubic matrix of GMO and cationic lipid DOTAP is proposed as an excellent host for siRNA molecules due to its ability to swell while retaining cubic structure [37].

Recently, a new colloidally stable lipoplex based on cubic LLC phase of monoolein has been developed by Zhen *et al.* [40]. This carrier system was functionalised with cationic lipids and showed a high delivery efficiency with low toxicity using a low cationic lipid-siRNA(N/P) ratio. Studies of hybrid cubic lipid vehicles for siRNA delivery have concentrated on physicochemical properties such as gene silencing efficiency, cytotoxicity and cellular uptake. Whilst several studies highlight the promising properties of lipid cubic phase carriers for delivery of siRNA, the biophysical aspects and interaction mechanisms of LNPs-siRNA need to be investigated. An understanding of the interaction mechanism and the release of siRNA from the cubosome is necessary in order to improve the *in vivo* siRNA transfer capability, reduce the cellular toxicity and increase the complex stability.

In this study, we demonstrate that complex of cubic phase forming lipid and cationic lipid with a biocompatible stabilizer such as Pluronic F127 have the potential to deliver siRNA independent of the charge ratio. In other words, siRNA can be added to a maximum concentration within cubosomes. We also found that siRNA was not released from the lipidic lipoplexes after exposure to acidic pH, which suggests that acidification of lipoplexes is not a significant factor in release of siRNA from our lipidic carrier.

DOTAP-phytantriol/siRNA complexes were prepared at different cationic lipid/siRNA charge ratios to characterize the interaction of cationic lipid and cubic phase lipids with siRNA. We used quartz crystal microbalance with dissipation (QCM-D) [49] and small angle X-ray scattering (SAXS) to investigate the biophysical aspects of binding and release of siRNA using free and immobilized cubosomes. Also, with the aim of providing insight into the correlation between phase behaviour of lipoplexes upon acidification and siRNA release, we investigated the effect of lower pH as found in endosomes on the structure of lipoplexes using QCM-D and SAXS measurements. Cationic lipid-siRNA complexes were prepared with low and high membrane charge and their size, ζ-potential, lyotropic mesophase behaviour, cell viability and gene silencing efficiency was characterized.

Results and Discussion

Physicochemical characterisation of DOTAP/Phytantriol LNPs and siRNA-lipoplexes. Dynamic light scattering (DLS) and ζ-potential measurements gave the mean particle size and surface charge of the DOTAP/Phytantriol LNPs and the siRNA lipoplexes, respectively. Table 1 summarizes the particle size, PDI and charge for the various lipid particles used in this study. DLS results indicated a mean particle size of 92 nm for 15 wt% DOTAP/Phy LNPs in PBS which form cubosomes and approximately 109 nm for the lipoplex with N/P ratios of 1 and 4 The polydispersity index (PDI) for the cubosome samples was approximately 0.2, which is comparable to reported values for related systems [45]. The data demonstrate that the introduction of buffer and siRNA to 15 wt% DOTAP-Phy solution resulted in a decrease in size and PDI as a result of a phase transition from lamellar to non-lamellar phases. Presumably, due to the charge shielding of the cationic DOTAP lipid head groups by the negatively charged phosphate in the buffer and the siRNA, this leads to an increase in the negative curvature of the interface so that cubic or hexagonal structures are more favourable. The more negatively curved interface will generate a cubic phase as previously reported for DDAB-Phy cubosomes [50].

Table 1. Particle size, ζ-potential, and SAXS data for DOTAP/Phy and DOTAP/Phy-siRNA lipoplexes.

Cationic lipid (wt%)/bulk lipid[a] formulation	N/P ratio[b]	Size (nm)	PDI	ζ-potential (mV)	SAXS[C]	Lattice parameter [d] (Å)
Phy-F127					Cubic (Pn3m)	70.5±0.02
15% DOTAP/Phy in water		914.7	1		Lα	
15% DOTAP/Phy in PBS		92.2	0.053	19.4	Cubic (Pn3m)	82.9± 1.3
15% DOTAP/Phy-siRNA	1	109.6	0.189	6.97	H_{II}	45.2±1.9
15% DOTAP/Phy-siRNA	2	109.1	0.191	11.7	H_{II}	45.0±1.5
15% DOTAP/Phy-siRNA	3	107.8	0.205	15.5	H_{II}	49.0±2.2
15% DOTAP/Phy-siRNA	4	104.2	0.243	17.1	H_{II}	44.8 ± 2.0

[a] The weight percent of cationic lipid in Phy was formulated at concentrations of 15 wt% of the total bulk lipid.
[b] N/P ratio is the molar ratio of the cationic lipid nitrogen (N) to siRNA phosphate (P) of the lipid particle formulations.
[c] Lyotropic mesophase (Lα: Lamellar phase, H_{II}: Inverse hexagonal phase).
[d] Lattice parameter measured via synchrotron SAXS analysis.

SAXS analysis (Fig. 1) showed that introduction of buffer (PBS) to 15 wt% DOTAP-Phy particles which are lamellar phase, promotes the formation of an inverse cubic phase with the *Pn3m* crystallographic space group. The SAXS spectrum of 15% DOTAP/Phy in water without siRNA displayed diffuse scattering and the absence of well-defined peaks, which is characteristic of a lipid vesicle system (lamellar phase). We observed that addition of siRNA with different charge ratios resulted in the formation of reversed hexagonal phases, which correlates well with previously reported data [12] for GMO/DOTAP systems. The amount of siRNA does not have a significant effect on the lattice parameter. Peaks shift to higher q and lower lattice parameter with addition of siRNA.

Immobilization of LNP-siRNA lipoplex on gold crystal surface. In order to study release of siRNA from LNPs, a multilayer immobilisation strategy was used to tether the lyotropic LNPs to the QCM chip surface as described previously [3]. 15 wt% DOTAP/Phy solutions in PBS, which form cubosomes based on our SAXS data, either containing bDSPE or not, were flowed over the NAv layer to interact with the modified surface. Table 2 shows the QCM frequency changes for each of the different cubosome compositions tested against the NAv surface.

Table 2. QCM-D data for NAv modified gold crystals with 15 wt% DOTAP/Phy solutions in PBS with different compositions

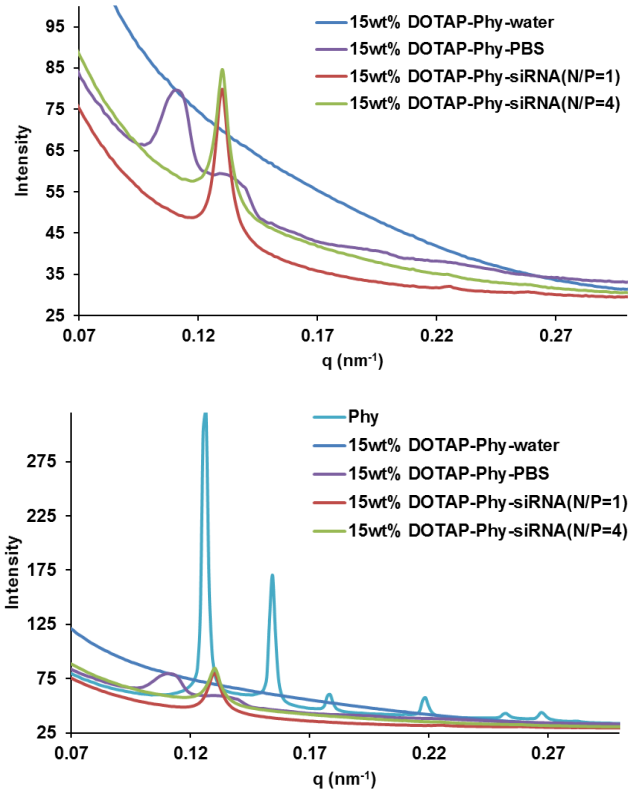

Figure 1. Synchrotron SAXS data for 15wt% DOTAP/Phy particles in water, devoid and containing siRNA N/P ratios of 1 and 4. Upper graph is expanded vertical scale.

Phytantriol LNPs without cationic DOTAP and bDSPE showed little interaction with the surface as demonstrated by the low frequency shift (-10 Hz) that was due to minimal non-specific adsorption. Similar nonspecific behaviour (Δf ≈ -19 Hz) was observed for the phytantriol/DOTAP LNPs devoid of bDSPE. For both LNPs samples containing bDSPE, around a 10-fold increase in the magnitude of the frequency change was observed, which showed greatly increased LNPs-surface interactions with the neutravidin coated surface (Fig. 2). This finding correlates well with previously reported data for phytantriol/bDSPE systems [20] which described a difference in frequency change as a function of the concentration and flow rate.

Cubosome composition	Δf (Hz)
Phy	-9.99
DOTAP-Phy	-18.90
bDSPE-Phy	-104.68
bDSPE-DOTAP/Phy	-127.15

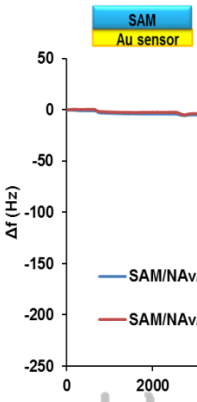

Figure 2. A QCM-D trace for binding of NAv and LNPs: traces show change in frequency (Δf) for the seventh harmonic of a given experiment flowed over an Au sensor surface at 25°C. At point (1), NAv is flowed into the chamber, and at point (2), (lipidic nanoparticles with or without biotin are flowed into the chamber.

Following immobilization of NAv on the sensor gold crystal, biotinylated LNPs (15 wt% DOTAP/Phy in PBS, which form cubosomes) were flowed into the QCM chambers to assess the level of surface coverage. A range of cubosome concentrations were titrated against the modified QCM surface to determine the optimal concentration for maximum surface coverage. Figure 3 shows the frequency and dissipation sensograms for different concentrations of bDSPE-15 wt% DOTAP/Phy cubosomes (from 0.025 μg/μL to 1 μg/μL). The 0.25, 0.5 and 1μg/μL cubosome solutions exhibited rapid binding kinetics with the surface but did not afford the highest frequency shift. Surprisingly, the maximum surface coverage (-260 Hz) was observed for the lowest concentration of cubosomes tested (0.025 μg/μL) with mild binding kinetics, indicating the specific binding with highest surface coverage.

The dissipation sensogram collected in parallel with the frequency sensogram did not show any post-deposition structural change or rearrangement, normally observed as a peak, indicating that the deposit was stable for all cubosome concentrations. This suggests that there is an optimal concentration for packing onto the modified surface, likely as the high cubosome concentrations coupled with the fast binding kinetics of the NAv-biotin interaction lead to

disordered cubosome binding, leaving small areas that are inaccessible to any more cubosomes. This is evidenced by decreased Δf for the higher cubosome concentrations.

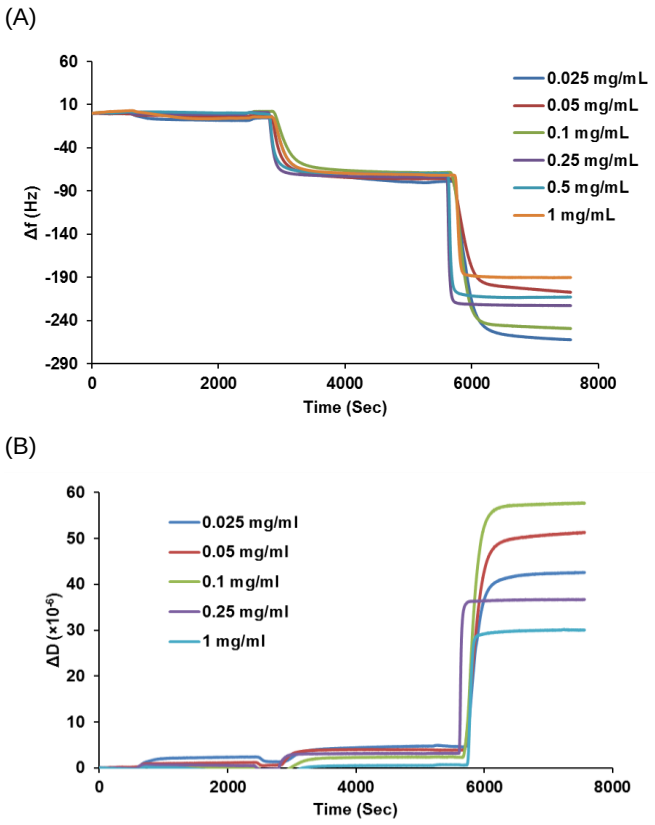

Figure 3. QCM-D traces of: (A) Δf, and (B) ΔD for different concentrations of bDSPE-15 wt% DOTAP/Phy LNPs. At point (1), NAv is flowed into the chamber, and at point (2), biotinylated LNPs were flowed into the chamber at concentrations between 0.025 -1 mg/mL.

Interaction of siRNA with positively charged cubosomes. To assess if the immobilized positively charged cubosomes are able to capture the payload, siRNA solutions in PBS (10 mM) were flowed into the QCM chamber over the immobilised cubosomes containing bDSPE-15 wt% DOTAP/Phy. QCM-D data (Fig. 4) indicated a discernible shift in frequency at the seventh harmonic upon interaction of siRNA with the positively charged cubosomes, indicating that siRNA binds to bDSPE-DOTAP/Phy cubosomes.

Viscoelastic modelling using Voigt formalism was performed to extract further details about the uptake process. The capture of siRNA was modelled as an adlayer as the simulation software is designed to calculate thicknesses of layer stacks; note that siRNA likely also adsorbed on the side and/or the internal cavities of the cubosomes.

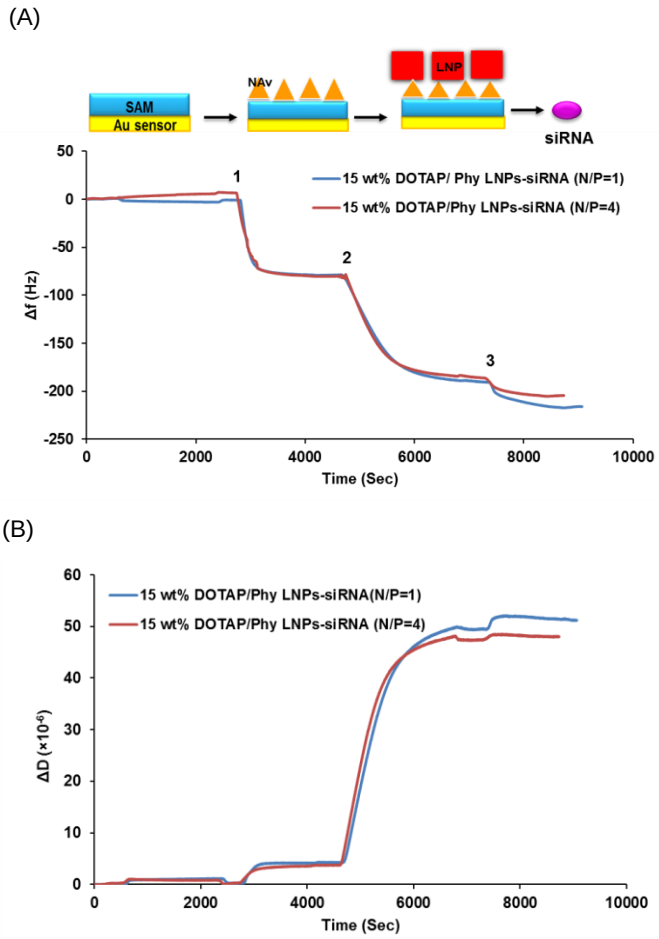

Figure 4. QCM-D traces of: (A) Δf, and (B) ΔD for capture of siRNA with different charge ratios onto the surface of the positively charged LNPs. At point (1), NAv is flowed into the chamber, at point (2), biotinylated lipidic nanoparticles are flowed into the chamber, and at point (3) siRNA solution in N/P ratios of 1 and 4 are flowed into the chamber.

Table 3 shows the frequency, dissipation, thickness and mass data for different N/P of siRNA interacting with the fixed concentration of biotinylated positively charged cubosomes (bDSPE-15 wt% DOTAP/Phy). The concentration of cubosomes is 0.025 mg/ml based on the concentration of DOTAP. The modelling yielded a thickness of 126 nm for the cubsomes and ~ 4 nm thickness for the

siRNA 'layer'. The corresponding mean particle size of the cubosome nanoparticles in water was approximately 92 nm by DLS measurements. This confirms that the bDSPE-15wt% DOTAP/Phy particles adsorbed onto the surface of the sensor crystals without a structural change. The size, however, was about 80 nm smaller than bDSPE/Phy characterized by Fraser *et al.* [1, 20], which suggests an effect of the cationic lipid and buffer solution on the cubosome structure and size. As expected, the mass of siRNA captured by the positively charged cubosomes with N/P ratio 1 was slightly higher than siRNA with N/P ratio 4. Moreover, the rapid kinetics of siRNA capture by the cubosomes, followed by smooth dissipation signals, indicates that siRNA is attached to the surface of the positively charged cubosomes and does not penetrate into the water channels.

Physical and interaction behaviour of siRNA preloaded within positively charged LNPs. The complex of siRNA-LNP (lipoplexes) were prepared as discussed in the Methods section. To investigate the physical and binding behaviour of siRNA preloaded within the DOTAP/Phy lipid particles, solutions of bDSPE-15 wt% DOTAP/Phy-siRNA with N/P = 1 and 4 were flowed onto the surface of the QCM crystals to interact with modified layer.

Table 3. QCM-D data for frequency and dissipation changes of the deposited layer on the surface of gold crystals[a]

Deposited Layer	Δf (Hz)	ΔD (×10^{-6})	Thickness (nm)	Mass (ng/cm^2)
NAv	- 77.5 ± 3.1	4.2 ± 0.7	21 ± 1.1	2284 ± 119
bDSPE-Phy	-122.4 ± 1	15.3 ± 2.2	50 ± 4	
bDSPE-15wt% DOTAP/Phy	-129 ± 18	52.0 ± 6.4	126 ± 3.3	13817 ± 368
siRNA (N/P=1) adsorbed onto positively charged cubosomes	- 22.4 ± 1.3	1.4 ± 0.8	3.7 ± 3.3	417 ± 41
siRNA (N/P=4) adsorbed onto positively charged cubosomes	- 16 ± 1.23	0.5 ± 0.3	2.6 ± 0.2	286 ±21

[a] Data were collected at 25°C and modelled using the Voigt formalism. The concentration of cubosomes was 0.025 mg/mL.

QCM-D sensograms (Fig. 5) showed larger frequency shift for siRNA preloaded within the positively charged LNPs indicating more mass due to siRNA addition. The samples with different charge ratios deposited onto the surface of crystals with similar frequency shifts but with slightly different kinetics. Dissipation values for all three deposits were similar, indicating that the introduction of siRNA does not have a substantial effect on the viscoelasticity of the cubosome layer. The output parameters of viscoelastic modeling (Table 4) indicated that mass and thickness of siRNA preloaded LNPs (lipoplexes) in different charge ratios were similar, indicating that charge ratio does not affect the structure of the LNPs. In other words, we can load a high amount of siRNA into the LNPs without compromising structure and delivery capability. Generally, increasing the cationic lipid to siRNA ratio can enhance stability and encapsulation efficiency of the lipoplex, but with an increased cytotoxicity [40]. Our data indicate that our positively charged LNPs are able to deliver siRNA with high efficiency and, hence, we examined their toxicity (see below).

Table 4. QCM-D data for frequency and dissipation changes of the deposited layer on the surface of gold crystals.

Deposited Layer	Δf (Hz)	ΔD (×10^{-6})	Thickness (nm)	Mass (ng/cm^2)
bDSPE-15wt% DOTAP/Phy	-129 ± 18	52 ± 6.4	126 ± 3.3	13817 ± 368
siRNA (N/P=1) preloaded within positively charged LNPs	-161 ± 14	48 ± 3.1	116 ± 4	12697 ± 506
siRNA (N/P=4) preloaded within positively charged LNPs	-155 ± 15	50 ± 2.2	124 ± 9.5	13608 ± 1051

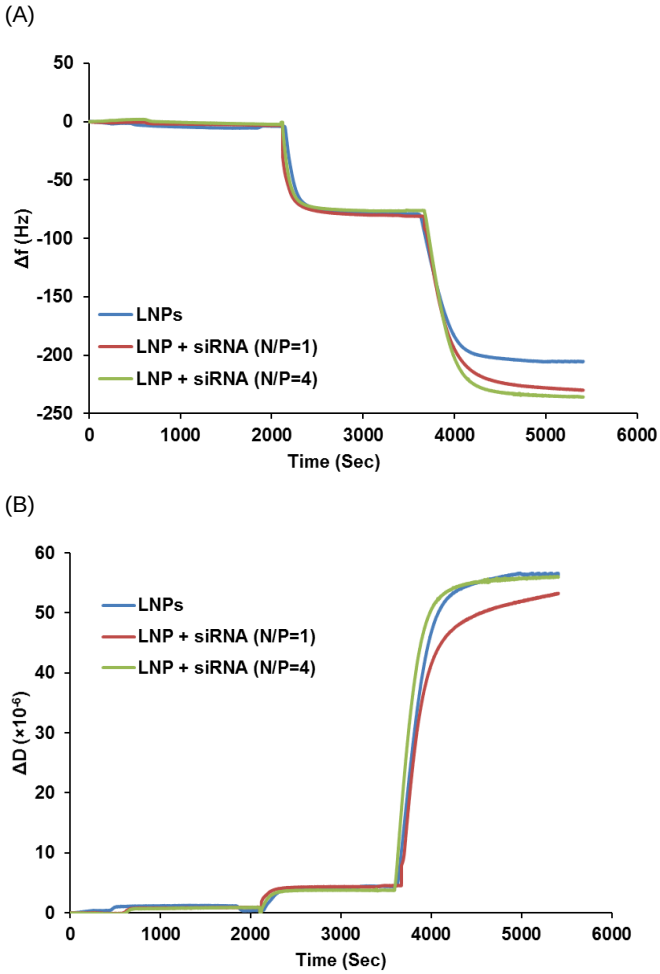

Figure 5. QCM-D traces of: (A) Δf, and (B) ΔD for positively charged LNPs with and without siRNA in different charge ratios deposited on the surface of modified crystals. At point (1) NAv (1 mM) was flowed into the chamber, and at (2) followed by flowing positively charged LNPs devoid and with siRNA

Biological studies. The amount of siRNA binding to 15 wt% DOTAP/Phy complexes and also the binding strength of siRNA with 15wt% DOTAP/Phy complexes was qualitatively valuated using gel electrophoresis stained with a nucleic acid specific dye. As seen in Figure 6, naked siRNA (lanes 1 and 3) easily migrates through the gel due to the small size and negative charge of the molecules and is observed toward the bottom of the gel. Because of the size and positive charge of the lipolexes, the siRNA was entrapped and no longer able to migrate freely through the gel. Therefore, the extent of siRNA binding can be approximated by the amount of free siRNA versus the amount retained at the top of the gel. As shown in Figure 6, lanes 2 and 4, the lipoplexes did not show complete siRNA binding neither with N/P ratio of 1 or 4 but more siRNA was bound at higher cationic lipid content, i.e. N/P=1, due to a stronger electrostatic interaction. These results would suggest that the amount of loosely bound siRNA decreased as the ratio of cationic lipid DOTAP to nucleic acid increased. However, substantial free siRNA remained in both cases, indicating saturation of the LNPs. Therefore, we examined LNP structure by SAXS.

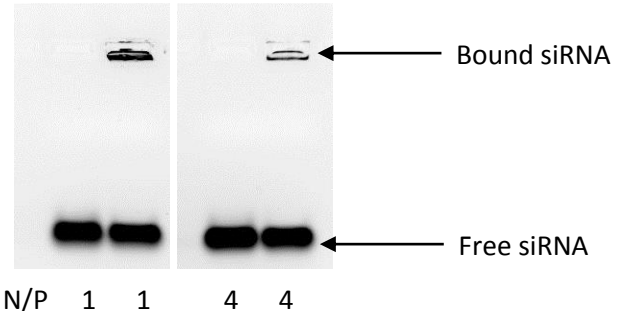

Figure 6. Gel electrophoresis of 15 wt% DOTAP/Phy complexes devoid and containing siRNA with N/P ratios of 1 and 4. Lanes 1 and 3 are siRNA and lanes 2 and 4 are LNP-siRNA lipoplexes.

Uptake of the loaded cubosomes by cells was also examined by confocal microscopy. siRNA labelled with [6'FAM] was bound to the lipid complex that contained or was devoid of Phytantriol labelled with R18. The addition of labelled siRNA dramatically increased the mean fluorescence, which indicated incorporation of the siRNA into the nanoparticles. Figure 7 shows confocal microscope images of 15wt% DOTAP/Phy with fluorescently labelled siRNA complexes. No particles were observed when a solution containing Phy-siRNA complex devoid of DOTAP was imaged (Fig. 7B). This indicates that addition of DOTAP significantly increased lipidic carrier and siRNA uptake as indicated by the increased red and green, respectively (Fig. 7A).

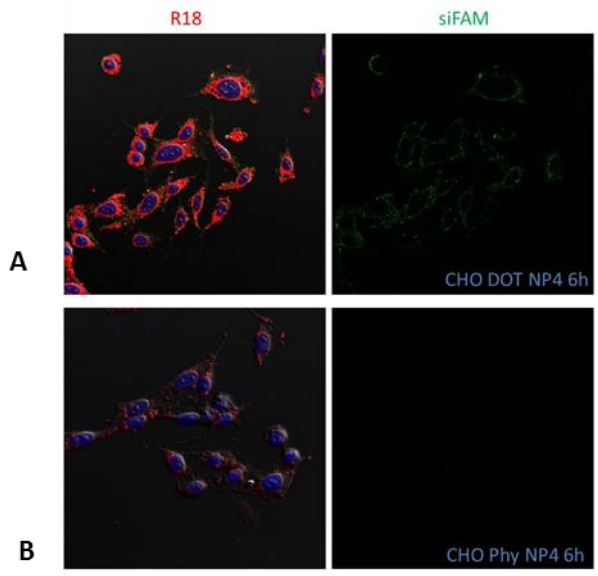

Figure 7. Fluorescent microscopy image of CHO cells with: (A) 15wt% DOTAP/Phy-siRNA, and (B) Phy-siRNA complexes (N/P = 4), after 6 h. Similar results seen for N/P=1. Scale bar is 25 μm.

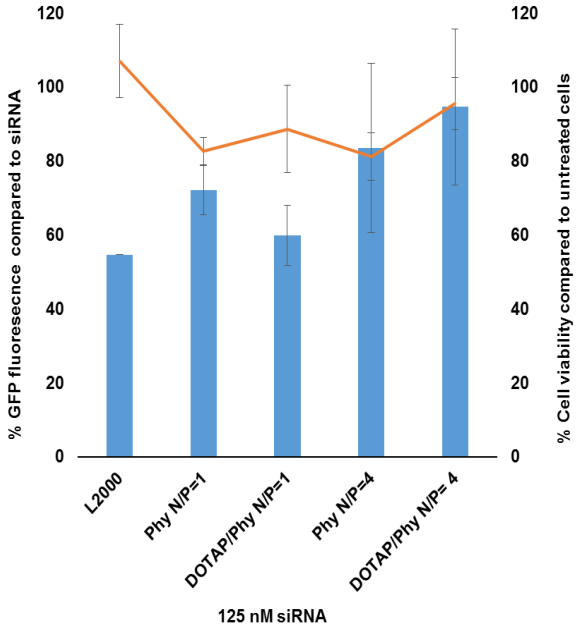

Figure 8. Cell viability results for CHO-GFP cells incubated with DOTAP/Phy-siRNA complexes (line) and GFP silencing in CHO cells (bars). The concentration of cationic lipid in the complexes was 15 wt% and N/P ratio of 1 and 4.

Gene-silencing experiments were performed to determine whether LNPs were efficient at delivering siRNA into the cells and, thus, inducing silencing of the reporter gene enhanced green fluorescent protein (GFP). GFP when excited by blue 408 nm laser emits a green signal at approximately 518 nm. CHO-GFP cells ubiquitously express GFP and successful delivery of siRNA targeting GFP to these cells can be determined by a shift in the cell population in a flow cytometry plot and by a decrease in mean GFP fluorescence. This is then analysed as a percentage knockdown compared to untreated control cells (Fig. 8). The result indicated that siRNA delivery was achieved with N/P=1. Interestingly, although cationic lipid-Phy containing complexes with different charge ratios formed similar inverted hexagonal phase particles, a trend of increasing knockdown with higher DOTAP (and more siRNA) content was observed. This correlates with the higher binding capacity of these compared to the N/P ratio 4 complexes. From these results, the amount of DOTAP and Phy did not appear to have an effect on the toxicity and, when there was a greater amount of siRNA, the release and silencing increased. However, further studies are required to confirm this observation.

Release of siRNA from LNPs under acidic conditions. Lipidic drug formulations are believed to enter cells by receptor-mediated endocytosis and the internalized complexes are retained in endosomes with no access to the cytoplasm, hence unable to initiate gene silencing [48].

We investigated the effect of the lower pH as found in endosomes of the structure of effective DOTAP-Phy/siRNA by QCM and high-resolution synchrotron SAXS, with the aim of providing insight into the correlation between phase behaviour of lipoplexes upon acidification and siRNA release. QCM raw data (Fig. 9) show that, upon introducing slightly acidic buffer (pH = 5.5) to the lipid particles either with and without siRNA, the frequency did not change significantly (Fig. 9A) i.e., the mass of the deposited layer did not change. However, in both cases there was a noticeable dissipation change (Fig. 9B), which indicated that the structure of positively charged cubosomes changed and the lipidic particles possibly became more structurally disordered in the acidic environment.

(A)

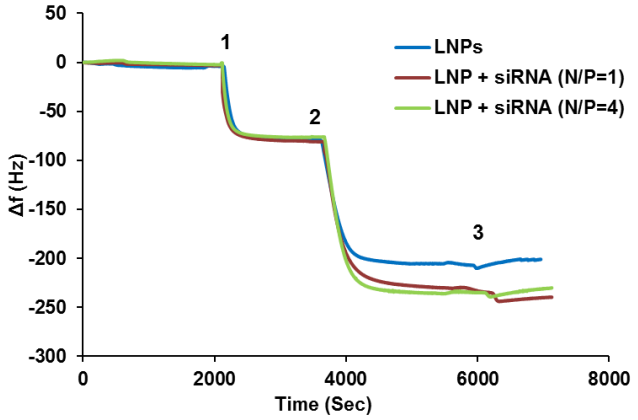

(B)

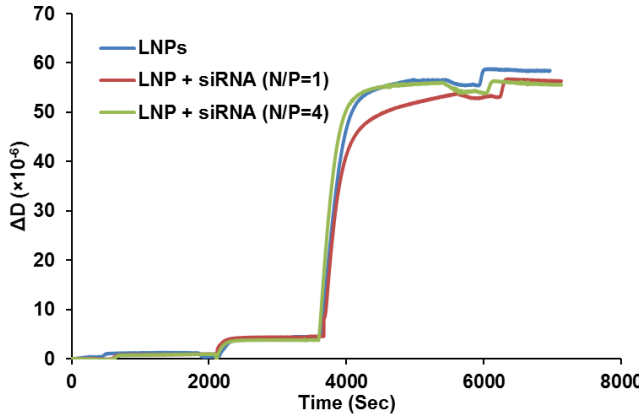

Figure 9. QCM-D traces of: (A) Δf, and (B) ΔD for positively charged LNPs devoid and containing siRNA with different charge ratios deposited on the surface of modified crystals. At point (1) NAv (1 mM) was flowed into the chamber, then (2) positively charged LNPs devoid and with siRNA were flowed into the chamber, and at point (3) buffer with pH=5.5 were flowed on the surface of deposited layers.

Figure 10 shows the SAXS patterns of DOTAP/Phy-siRNA lipoplexes with N/P ratios of 1 and 4 at pH values: 7.4, 6.5, 6 and 5.5. At pH 7.4, lipoplexes form a mixture of hexagonal and lamellar phases, which is indicated by the appearance of peaks in the scattering data consistent with the formation of hexagonal and lamellar liquid crystalline structures. Upon lowering the pH from pH 7.4 to pH 5.5, the SAXS pattern of the lipoplexes changed, but the hexagonal and lamellar structures of the lipoplexes were essentially preserved with siRNA, remaining tightly bound to the lipid bilayers, and for both charge ratios the diffraction peaks remained constant. Despite better siRNA binding with DOTAP not much difference in silencing was observed at either N/P ratio between Phy alone and 15wt% DOTAP – most likely due to a lack of siRNA release as observed in these assays, and indicating that DOTAP is unlikely to be the most efficient cationic lipid to be utilised in this system. Development of new lipidic nano-carrier components that improved loading and that bind the siRNA less strongly to improve release, will greatly improve delivery with these vehicles. Work towards this is ongoing.

(A)

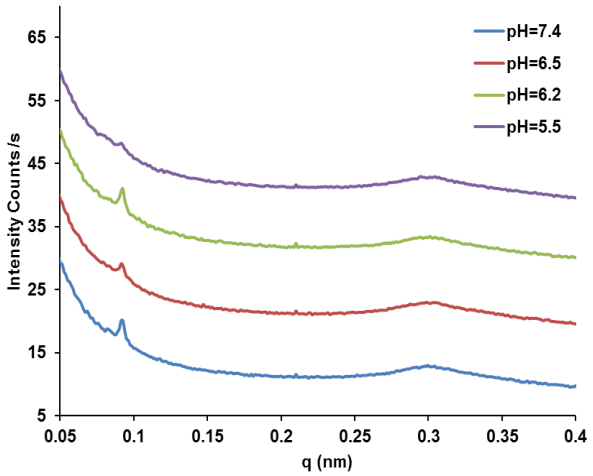

(B)

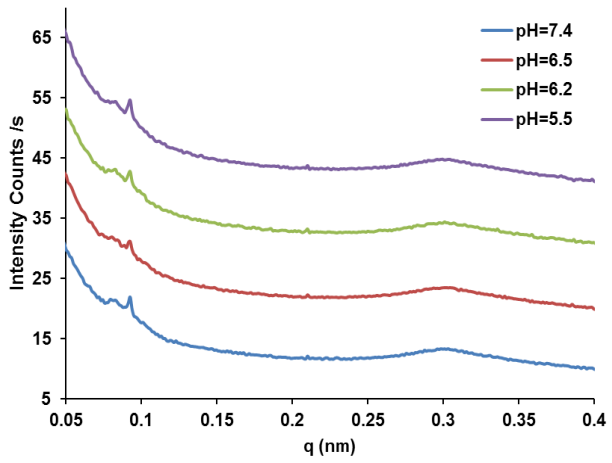

Figure 10. SAXS diffractograms in buffer at different pH of: (A) Phy-DOTAP/siRNA lipoplexes with N/P ratio 1, and (B) Phy-DOTAP/siRNA lipoplexes with N/P ratio 4.

Conclusions

In the present study, we investigated the binding of siRNA to positively charged lipidic particles in the form of non-lamellar mesophases, the extent of siRNA release, the efficiency of lipidic particles in siRNA delivery, and structural changes of lipoplexes upon acidification. The results show QCM-D as a useful method for studying the binding and release of therapeutic agents from the lipidic carriers. This technique can help develop and understand the importance of siRNA binding on the outside versus internalised in nano-carrier pores and its release from these vehicles for improved siRNA delivery efficiency. Essential physicochemical parameters of the cationic LNP/siRNA lipoplexes, such as particle size, lyotropic mesophase behavior, cytotoxicity, gene silencing and uptake efficiency, were characterized. The cationic carriers were able to induce gene silencing and the acidic conditions of the endosome were not a significant factor in the release of siRNA from the cationic lipidic carriers.

Experimental Section

Materials. 11-mercaptoundecanoic acid (MUA, 99%), 6-mercapto-1-hexanol (97%), N-ethyl-N-(3-dimethylaminopropyl) carbodiimide) (EDC), and N-hydroxysulfosuccinimide (NHS) were purchased from Sigma Aldrich (St Louis, USA). 1,2-Distearoyl-sn-glycero-3-phosphoethanolamine-N-[biotinyl(polyethyleneglycol)-2000] (ammonium salt, 100%) (bDSPE) and 1,2-dioleoyl-3-trimethylammonium-propane (chloride salt) (DOTAP) were purchased from Avanti Polar Lipids Inc. (Alabaster, USA). Neutravidin (NAv) was purchased from Thermo Fisher Scientific (Waltham, USA). Phosphate buffered saline (PBS) tablets, 3,7,11,15-tetramethyl-1,2,3-hexadecanetriol (phytantriol) (96%), and Pluronic F127 (poly(ethyleneoxide)-poly(propyleneoxide)-poly(ethyleneoxide) (PEO-PPO-PEO)) were purchased from Sigma Aldrich. Chloroform, hydrogen peroxide (30% GR for analysis ISO) and ethanol (100%) were purchased from Merck (Beeston, UK). Ammonia solution (28% analytical Univar Reagent) was purchased from Ajax Finechem (Sydney, Australia). These chemicals were used as received without further purification.

siRNA duplexes. Anti-GFP and negative control siRNAs were obtained from QIAGEN (USA). The anti-GFP siRNA sequence is sense 5' GCAAGCUGACCCUGAAGUUCAU 3' and antisense 5' GAACUUCAGGGUCAGCUUGCCG 3'. The nonsilencing control siRNA sense sequence was 5' UUCUCCGAACGUGUCACGUDTDT 3' and antisense is 5' ACGUGACACGUUCGGAGAADTDT 3'. This is a valid negative control with no homology to any known mammalian gene [40].

Preparation of lipidic particles. Cationic lipidic particles containing DOTAP and phytantriol were prepared by co-solubilizing 200 mg of phytantriol in a 20 ml glass vial with a calculated set amount of cationic lipid (DOTAP) and Pluronic F127 (10% w/w of phytantriol) dispersant in chloroform. Where required in QCM experiments, bDSPE (0.5% w/w) of phytantriol lipid) was added to mixtures. The mixtures were vortex-mixed thoroughly and the chloroform removed by rotary evaporation for 2 h. The mixtures were freeze-dried overnight to complete chloroform removal. The mixtures were heated at 50°C to melt the lipid Pluronic mixtures and 4 ml of Milli-Q water was added prior to dispersion by ultrasonication (Misonix Sonicator S-4000 attached with a misonix microtip 418) for 10 minutes in pulse mode (5 s pulse with 5 s break) at 75% of maximum power, resulting in homogenous transparent dispersion. The final concentration was 15 wt% DOTAP of total lipid material. Dispersions were stored at 25°C for 24 h prior to further experimentation to enable equilibration of lipid, Pluronic F127 and water [40]. The dispersions were combined with 100 mM phosphate saline buffered (PBS) at the volume ratio of 1 to 2.

Preparation of siRNA-lipoplexes. siRNA lipoplexes were prepared with various charge ratios (N/P: positively charged nitrogen (DOTAP) to negatively charged phosphate (siRNA)). Typically, the siRNA (1.2 µg/µl) in PBS (10 mM) was added to 0.025 µg/µl of 15 wt% DOTAP-phytantriol, with the total lipid concentration adjusted to achieve the desired cationic lipid-siRNA ratio. Solutions were immediately vortexed

following addition of siRNA to allow for homogenous mixing. N/P ratios of 1 and 4 were used in this study.

Dynamic light scattering (DLS) and zeta (ζ) potential measurements. The particle diameter distribution, polydispersity index (PDI), and surface charge of lipidic particles and siRNA-lipoplexes were obtained from triplicate DLS measurements using a Nano-ZS Zetasizer (Malvern Instruments, UK). Measurements were made at 25°C after diluting the lipid particle dispersions in 10 mM PBS. ζ potential was measured using zeta potential cells after diluting particles in 10 mM HEPES buffer.

Synchrotron SAXS. Small angle X-ray scattering (SAXS) experiments were performed at 37ºC in 1.0 mm quartz capillaries using the SAXS/WAXS beamline at the Australian Synchrotron. A wavelength of 1.24 Å was employed to record 2D SAXS image pattern using a Pilatus 1M CCD camera. A measurement time of 1 s was employed minimize beam damage. A silver behenate standard was used to calibrate the reciprocal space vector. Sample temperature was controlled a recirculating bath (Julabo-Germany) with arrange of accessible temperatures. Two dimensional diffraction images were record on a Mar CX165 detector with analysis in the q range 0.017-0.645 $Å^{-1}$. Data reduction (calibration and integration) was performed using AXcess, a custom designed SAXS analysis program written by Dr Andrew Heron, Imperial College, London [40]. MES buffer with 150 mM NaCl was used to study the effect of acidic condition on the release of siRNA.

Quartz crystal microbalance (QCM-D) measurements. QCM-D measurements were performed with a Q-Sense E4 system (Q-Sense, Västra Frölunda, Sweden) to monitor cubosome-siRNA binding and release in real time. Multilayer strategies developed by Vermette *et al*. [36] and Fraser *et al.* [20] were used to permit capture of cubosomes onto chemically modified QCM crystals. The covalent attachment of NAv onto the sensor surface immobilised by self-assembled monolayer (SAM) layer was used for deposition of cubosome and siRNA. The presence of NAv enables specific tethering of functionalised cubosomes to the sensor surface via biotin binding, which results in a thin and mechanically stable layer [32, 42]. The relation between the mass of each respective layer deposited (ng/cm^2) and the corresponding frequency change is described by Sauerbery equation:

$$\Delta m = -\frac{\mathrm{C}}{\mathrm{n}}\Delta f \qquad (1)$$

where C (17.7 ng/cm^2 at f = 5 MHz) is the mass sensitivity constant and n (1, 3, 5 or 7) is the Eigenmode or overtone number [43]. According to Sauerbrey there is a linear relation between the frequency and mass and this equation is only valid for rigid, uniform films with low energy dissipation on the surface of QCM crystal [44].

In most situations the adsorbed layer is viscoelastic, for which the Voigt model is applicable. The model relates the dampening of the crystal oscillation, measured as dissipation (eq. 2), to viscosity of the adsorbed layer on the QCM-D sensor surface and the shear modulus. The energy dissipation of the crystal oscillation gives insight into the viscoelasticity (film's softness) of the adsorbed layer and is calculated from [45]:

$$D = \frac{E_{lost}}{2\pi E_{stored}} \qquad (2)$$

where D is the dissipation of the layer, E_{lost} is the energy lost during one oscillation cycle, and E_{stored} is the total energy stored in the oscillation. The Voigt model used in this work assumes a homogenous layer (i.e., height and thickness) in complete surface coverage.

Preparation and surface modification of the QCM-D sensors. The QCM-D sensor crystals were rinsed with ethanol and dried under a gentle stream of N_2 gas, after which they were placed in a 1:1:3 mixtures of ammonium hydroxide solution (28%), hydrogen peroxide (30%), and Milli-Q water, at 75°C for 20 min. The crystals were then rinsed with Milli-Q water and ethanol, and dried under a gentle stream of N_2 gas. Following cleaning the chips were immersed in binary mixtures of 2.5 mM 11-mercaptoundecanoic acid (MUA) and 7.5 mM mercaptohexanol in absolute ethanol for 24 h. Chips were then rinsed with ethanol, dried under a stream of N_2 gas, and immediately inserted into the QCM chamber.

To immobilise NAv to the surface of modified crystals, the SAM surfaces were activated *in situ* by treating the SAM-modified crystals with 46 mM of EDC/NHS for 1 h to produce

a carboxyl terminated surface [20]. The biotin-NAv binding interaction was employed due to the strong binding interaction. The gold sensor modified by SAM of alkanethiols is suggested to achieve the highest surface coverage due to chemisorption of thiol groups onto the gold surface via the formation of thiolate–metal bonding [46-47]. SAMs can provide a robust and reproducible method of fabricating immobilised layers and provide long-term stability/functionality. Therefore, covalent attachment of NAv to SAM was chosen as immobilisation matrices for biotinylated cubosome deposition. For immobilizing of NAv, the SAM prepared from COOH- and OH- terminated alkane thiols were activated *in situ* by treating the modified crystals with 46 mM of EDC/NHS for 1 h to convert carboxylic acid to NHS ester group. After activation, surfaces were immediately modified by flowing a solution of PBS pH 7.4 containing NAv (1 µM) at flow rate 30 µL/min at 25°C. Samples were then rinsed in PBS buffer pH 7.4 before immobilising further layers.

Agarose gel electrophoresis. Samples containing 50 pmol of siRNA were electrophoresed on a 2% agarose in 1TBE (89 mM Tris base, 89 mM boric acid, 2 mM EDTA) at 100 V for 40 min. siRNA was visualised by gel red (Jomar Biosense) on a UV transilluminator with camera, the image was recorded by the GeneSnap program (Syngene, USA) [40].

Cell line and culture conditions. Chinese hamster ovary cells constitutively expressing green fluorescent protein (CHO-GFP) (kindly received from K. Wark, CSIRO, Australia) were grown in MEMα modification supplemented with 10% fetal bovine serum, 10 mM HEPES, 0.01% penicillin, and 0.01% streptomycin at 37°C with 5% CO_2 and subcultured twice weekly. Human embryonic kidney cells (HEK293) cells were grown in RPMI1640 supplemented with 10% fetal bovine serum, 10 mM HEPES, 2 mM glutamine, 0.01% penicillin, and 0.01% streptomycin at 37°C with 5% CO_2 and subcultured twice weekly [48].

SiRNA particle visualization. Samples were prepared as described above with either siRNA or siRNA labelled with [6'FAM]. Samples were mounted in Prolong Gold on microscope slides and covered with coverslips. Slides were imaged with Leica SP5 confocal microscope.

Cell cytotoxicity assay. CHO-GFP and HEK293 cells were seeded at 1 × 10^4 cells in 96-well tissue culture plates in triplicate and grown overnight at 37°C with 5% CO_2. GMO−siRNA complexes were added to cells and incubated for 72 h in 200 µL standard media. Toxicity was measured using the Alamar Blue reagent (Invitrogen USA) according to manufacturer's instructions. Briefly, 20 µL of Alamar Blue was added to each well and incubated for 4 h at 37°C with 5% CO2. The assay was read on a EL808 absorbance microplate reader (BIOTEK, USA) at 540 and 620 nm. Cell viability was determined by subtracting the 620 nm measurement from the 540 nm measurement. Results are presented as a percentage of untreated cells [40].

G*ene silencing assay*. CHO-GFP cells were seeded at 1 × 10^4 cells in 96-well tissue culture plates in triplicate and grown overnight at 37°C with 5% CO_2. For positive and negative controls, siRNAs were transfected into cells using Lipofectamine 2000 (Invitrogen, USA) as per manufacturer's instructions. Briefly, 50 pmol of the relevant siRNA were mixed with 1 µL of Lipofectamine 2000 both diluted in 50 µL of OPTI-MEM (Invitrogen, USA) and incubated at room temperature for 20 min siRNA:Lipofectamine mix was added to cells and incubated for 4 h. Cell media was replaced and incubated for 72 h. For cationic lipid/Phy-siRNA complexes, cell media was removed and replaced with 100 µL of OPTI-MEM. Cationic lipid/Phy-siRNA complexes formulations were added to cells and incubated for 4 h. Media was replaced to standard growth media and incubated for a further 72 h. Cells were washed twice with PBS, trypsinized, and washed once with FACS wash (PBS with 1% FBS). Cells were subjected to flow cytometry, and EGFP silencing was analyzed as percentage of the nonsilencing siRNA or cubosome mixture without siRNA mean EGFP (measured on FITC wavelength) fluorescence [48].

Acknowledgements

B.T.-A. acknowledges the University of Melbourne and the CSIRO for a joint studentship.

Keywords: cubosomes, siRNA, lipid mesophase, QCM-D, drug release

[1] S. Fraser, F. Separovic, A. Polyzos, *Eur. Biophy. J*. **2009**, 39, 83-90.
[2] J.C. Shah, Y. Sadhale, D.M. Chilukuri, *Adv. Drug Delivery Rev*. **2001**. 47, 229-250.
[3] D. McLoughlin, M. Imperor-Clerc, D. Langevin, *ChemPhysChem*. **2004**, 5, 1619-23.
[4] E. Esposito, R. Cortesi, M. Drechsler, L. Paccamiccio, P. Mariani, C. Contado, E. Stellin, E. Menegatti, F. Bonina, C. Puglia, *Pharm Res.* **2004**, 22, 2163-73.
[5] a) V. Luzzati, A. Tardieu, T.C. Krzywicki, E. Rivas, F.R. Husson, *Nature*. **1968**, 220, 485-488; b) Z. Karami, M. Hamidi, *Drug Discov Today*., **2016**, 21(5):789-801.
[6] M.J. Lawrence, *Chem. Soc. Rev.* **1994**, 417-424.
[7] H. Kim, C. Leal, *ACS Nano*, **2015**, *9*, 10214–10226.
[8] A.D. Benedicto, D.F. O'Brien, *Macromolecules*. **1997**, 30, 3395-3402.
[9] Y. Chen, P. Ma, S. Gui, *Biomed. Res. Int*. **2014.** 2014, 1-12.
[10] L. Barauskas, M. Johnsson, F. Joansson, F. Tibers, *Langmuir*. **2005**. 21, 2569-2577.
[11] Z. Yang, X. Peng, Y. Tan, M. Chen, X. Zhu, M. Feng, Y. Xu, C. Wu, *J. Nanomater*. **2011**, 2011, 1-10.
[12] P.T. Spicer, K. L. Hayden, M. L. Lynch; A. Ofori-Boateng, J. L. Burns, *Langmuir*. **2001**, 17, 5748–5756.
[13] R. Negrini, R. Mezzenga, *Langmuir*. **2011**. 27, 5296-5303.
[14] X. Mulet, B.J. Boyd, C.J. Drummond, *J. Colloid Interf. Sci*. **2013**, 393, 1-20.
[15] R. Negrini, R. Mezzenga, *Langmuir*. **2012**, 28, 16455-62.
[16] S.B. Rizwan, B.J. Boyd, T. Rades, S. Hook, *Expert. Opin. Drug Deliv*. **2010**, 7, 1133-44.
[17] M.G. Lara, M. Vitoria, L.B. Bentley, J.H. Collett, *Intern. J. Pharmaceut*. **2005**, 293, 241-250.
[18] J. Clogston, G. Craciun, D.J. Hart, M. Caffrey, *J. Control Release*. **2005**, 2, 441-61.
[19] S.B. Rizwan, T. Hanley, B.J. Boyd, T. Rades, S. Hook, *J. Pharm. Sci*. **2009**. 98, 4191- 204.
[20] S.J. Fraser, R.M. Dawson, L.J. Waddington, B.W. Muir, X. Mulet, P.G. Hartley, F. Separovic, A. Polyzos, *Aust. J. Chem.* **2011**. 64, 46-53.
[21] A. Angelova, B. Angelov, R. Mutafchieva, S. Lesieur, P. Couvreur, *Acc. Chem. Res*. **2011**, 44, 147-156.
[22] B. Angelov, A. Angelova, S.K. Fillipove, T. Narayanan, M. Drechsler, P. Stepanek, P. Couvreur, S. Lesiur, *J. Phys. Chem. Lett*. **2013**, 4, 1959-1964.
[23] B. Angelov, A. Angelova, M. Drechsler, V. M. Garamus, *Soft Matter.* **2015**, 11, 3686-3692.
[24] A. Angelova, B. Angelov, R. Mutafchieva, S. Lesieur, *J. Inorg. Organomet. Polym.* **2015**, 25, 214-232.
[25] A. Angelova, B. Angelov, M. Drechsler, S. Lesieur, *Drug Discov. Today.* **2013**, 18, 1263-1271.
[26] Y. Sadhale, J.C. Shah, *Pharm. Dev. Technol*. **1998**. 3, 549-556.
[27] F. Takeshita, T. Ochiya, *Cancer Sci*. **2006,** 9, 689-96.
[28] D.V. Morrissey, J. A. Lockridge, L. Shaw, K. Blanchard, K. Jensen, W. Breen, K. Hartsough, L. Machemer, S. Radka, V. Jadhav, N. Vaish, S. Zinnen, C. Vargeese, K. Bowman, C.S. Shaffer, L.B. Jeffs, A. Judge, I. MacLachlan, B. Polisky, *Nature Biotechnol*. **2005**, 23, 1002-1007.
[29] S.J. Tan, P. Kiatwuthinon, Y.H. Roh, J.S. Kahn, D. Luo, *Small.* **2011**, 7, 841-856.
[30] K.A. Whitehead, R. Langer, D.G. Anderson, *Nat. Rev. Drug Discov*. **2009**. 8, 129-138.
[31] C.L. Walsh, J. Nguyen, M.R. Tiffany, F.C. Szoka, *Bioconjugate Chem*. **2013**. 24, 36-43.
[32] Y.-C. Tseng, S. Mozumdar, L. Huang, *Adv. Drug Delivery Rev.* **2009**. 61, 721-731.
[33] K. Buyen, S.C. De Smedt, K. Braeckmans, J. Demeester, L. Peeters, L.A.V. Grunsven X.D.M. Du Jeu, R. Sawant, V. Torchilin, K. Farkasove, M. Ogris, N.N. Sanders, *J. Control. Release.* **2012**. 158, 362-370.
[34] A. Schroeder, C.G. Levins, C. Cortez, R. Langer, D.G. Anderson, *J. Intern. Med*. **2010**, 267, 9-21.
[35] D. Bhavsar, K. Subramanian, S. Sethuraman, U.M. Krishnan, *Curr. Gene Ther.* **2012**, 12, 315-332.
[36] P. Vermette, L. Meagher, E. Gagnon, H.J. Griesser, C.J. Doillon, *J. Control. Release*. **2002**, 80, 179-195.
[37] C. Leal, N.F. Bouxsein, K.K. Ewert, C.R. Safinya, J. *Am. Chem. Soc*. **2010**. 132, 16841-47.
[38] Z.A. Almsherqi, S.D. Kohlwein, Y. Deng, *J. Cell. Biol.* **2006**, 19, 839- 44.
[39] Z. Almsherqi, S. Hyde, M. Ramachandran, Y. Deng, *J. R. Soc. Interface*. **2008**, 5, 1023-29.
[40] G. Zhen, T.M. Hinton, B.W. Muir, S. Shi, M. Tizard, K.M. McLean, P.G. Hartley, P. Gunatillake, *Mol. Pharmaceut*. **2012**, 9, 2450-2457.
[41] H. Brochu, P. Vermette, *Langmuir*. **2007**, 23, 7679-86.
[42] X. C. Zhou, L.Q. Huang, and S.F.Y. Li, *Biosens. Bioelectron*. **2001**, 16, 85-95.
[43] G. Sauerbrey, *Z. Phys.* **1959**, 155, 206-222.
[44] K. A. Marx, *Biomacromolecules*. **2003**, 4, 1099-1120.
[45] F. Höök, B. Kasemo, *Anal. Chem,* **2001**. 73, 5796-5804.
[46] J.J. Gooding, D.B. Hibbert, *Trends Anal. Chem*. **1999**, 18, 525-533.
[47] M. Seifert, M.T. Rinke, H.J. Galla, *Langmuir*. **2010**, 26, 6386-93.
[48] G. Sahay, W. Querbes, C. Alabi, A. Eltoukhy, S. Sarkar, C. Zurenko, E. Karagiannis, K. Love, D. Chen, R. Zoncu, Y. Buganim, A. Schroeder, R. Langer, D.G. Anderson, *Nature Biotech*. **2013**, 31, 653-661.
[49] C. Zhou, J.M. Friedt, A. Angelova, K.H. Choi, W. Laureyn, F. Frederix, L. A. Francis, A. Campitelli, Y. Engelborghs, G. Borghs, *Langmuir*. **2004**, 20, 5870-5878.
[50] B.W. Muir, G. Zhen, P. Gunatillake, P.G. Hartley, *J. Phys. Chem B*. **2012**. 116, 3551-56.

Entry for the Table of Contents:

ARTICLE

Releasing siRNA: Binding and release of short interfering ribonucleic acid (siRNA) from lyotropic liquid crystalline lipid nanoparticles (LNPs) on a self-assembled monolayer was demonstrated by quartz crystal microbalance. SAXS was used to characterise the attached LNPs.

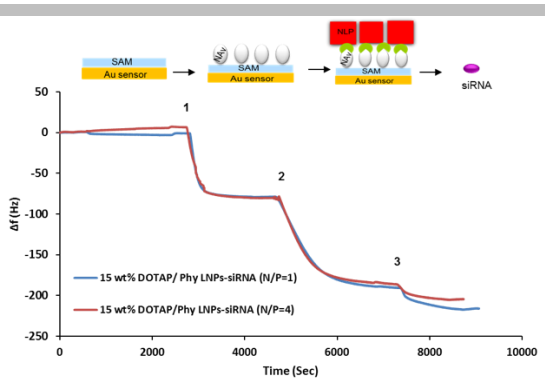

*B. Tajik-Ahmadabad, A. Mechler, B.W. Muir, K. McLean, T.M. Hinton, F. Separovic, A. Polyzos**

Page No. – Page No.

A QCM-D and SAXS Study of the Interaction of Functionalised Lyotropic Liquid Crystalline Lipid Nanoparticles with siRNA